Next Nanotechnology 10 (2026) 100591

Contents lists available at ScienceDirect

Next Nanotechnology

journal homepage: www.sciencedirect.com/journal/next-nanotechnology

Short communication

Probing back contact interfaces and hole tunneling in Cu_2ZnSnS_4 solar cells using temperature-dependent J–V curves

Jüri Krustok [a,*], Raavo Josepson [b], Achmad Nasyori [a], Marit Kauk-Kuusik [a]

[a] Department of Materials and Environmental Technology, Tallinn University of Technology, Ehitajate tee 5, Tallinn 19086, Estonia
[b] Division of Physics, Tallinn University of Technology, Ehitajate tee 5, Tallinn 19086, Estonia

ARTICLE INFO

Keywords:
Kesterites
Solar cells
Back contact
Hole tunneling
Temperature dependence

ABSTRACT

The temperature-dependent behavior of the short-circuit current density J_{SC} in Cu_2ZnSnS_4 (CZTS) thin-film and monograin layer solar cells was investigated over a wide temperature range (20–320 K) to clarify the properties of the back contact. All measured $J_{SC}(T)$ characteristics exhibited a distinct S-shaped dependence, indicating the presence of a transport barrier at the back interface. A modified Pöschl–Teller potential barrier model, which captures the temperature-dependent tunneling of holes, was successfully used to describe this behavior. Furthermore, spatial inhomogeneities at the back contact were identified, and the obtained data can be described by a Gaussian distribution of barrier heights across the interface.

1. Introduction

Kesterite-based thin-film solar cells, most commonly employing $Cu_2ZnSn(S,Se)_4$ (CZTSSe) or Cu_2ZnSnS_4 (CZTS) absorbers, are promising photovoltaic devices composed of earth-abundant and non-toxic elements. The current record efficiency of CZTS is 13.2%, and the CZTSSe kesterite cells show efficiency of 16.6%. [1] However, their performance remains limited by non-ideal recombination and carrier transport mechanisms, many of which originate from bulk band tailing and interface-related barriers. [2,3] In particular, the back contact as a Schottky junction between metal and CZTS has been repeatedly identified as a critical interface where band misalignment, secondary phases, or defect-induced dipoles can give rise to an extraction barrier that limits carrier collection. [4,5] Temperature-dependent photocurrent measurements provide a powerful method for probing such barriers. Under short-circuit conditions, the current density J_{SC} is determined by the balance between photogeneration and carrier collection. It is shown that the typical Mo/CZTS back contact of kesterite solar cells includes a beneficial MoS_2 thin layer, and this layer makes the back contact even more complicated. [6] In the absence of transport limitations, one expects only a weak temperature dependence of short circuit current J_{SC}. Typically, J_{SC} decreases slightly at low temperatures due to bandgap widening and reduced absorption near the band edge. However, at lower temperatures, the carrier mobility becomes essential. It is known that CZTS is a highly defective material with quite deep potential fluctuations. These valence band potential wells can effectively trap holes, which decreases both hole mobility and Jsc. For a spatially uniform barrier, this would lead to a monotonic and strongly activated temperature dependence of J_{SC}. Schottky barrier is always composed of two contributions: thermionic emission and the tunneling process. Thermionic emission is highly sensitive to both the barrier height and temperature. [7] Strong electric fields can effectively thin the barrier, enabling carriers to tunnel through it, whereas higher temperatures facilitate carrier transport over the barrier. In this work, we investigate the temperature dependence of J_{SC} in CZTS solar cells over the range 20–320 K. We observe a pronounced S-shaped behavior that deviates strongly from the simple exponential thermionic emission model. Furthermore, we find that solar cells fabricated with different back contact materials exhibit systematic variations in the shape and slope of the $J_{SC}(T)$ dependencies.

2. Experimental details

For a more detailed analysis of $J_{SC}(T)$ dependencies, we selected four different CZTS solar cells. Two of them were thin-film (TF) solar cells, and two were monograin layer (MG) solar cells. Each cell category includes one high-performing cell and one with lower performance. This cell selection was made in order to examine the changes in the $J_{SC}(T)$ dependences of CZTS solar cells with widely disparate characteristics as well as of back contacts prepared differently. Fig. 1(a) shows the *J-V*

* Corresponding author.
E-mail address: juri.krustok@taltech.ee (J. Krustok).

https://doi.org/10.1016/j.nxnano.2026.100591
Received 18 April 2026; Received in revised form 12 June 2026; Accepted 29 June 2026

curves for each cell, and obtained parameters can be found in Table 1.

As an illustration, we also show the temperature dependence of the TF2 cell's *J-V* curves in Fig. 1(c). All room-temperature *J-V* curves were measured under standard test conditions (AM 1.5, 100 mWcm^{-2}). A halogen lamp was employed for low-temperature measurements. Temperature-dependent *J-V* measurements were carried out in the temperature region from 20 K to 320 K by using a closed-cycle helium cryostat (Janis CCS−150). The temperature was adjusted up to RT via a temperature controller (LakeShore Model 335). Janis cryostat typically achieve temperature stabilization accuracies of ±50 mK or better. J_{SC} vs T curves are presented in Fig. 1(b). Every curve exhibits a characteristic S-shaped behavior.

Thin-film solar cells with the structure Mo/CZTS/CdS/i-ZnO/ITO were fabricated using a spin-coated CZTS absorber prepared in ambient air from DMSO-based precursors. Mo- coated soda lime glass was used as a substrate. Then, the sulfurization process was carried out in a graphite box containing 200 mg of sulfur, using an OTF−1200X tube furnace. The temperature was ramped to 650 °C within 33 min and held at the target temperature for 20 min under an Ar atmosphere at a pressure of 8×10^2 Torr. During this process, a thin MoS_2 layer was formed between the Mo substrate and the CZTS absorber. Post-annealing of the complete devices was conducted in air on a hot plate at 300°C for different times using a graphite box. The CZTS absorber layer thickness in TF solar cells ranged from 800 and 1200 nm thick. Further details on TF solar cell preparation can be found in [8]. CZTS monograin layer solar cells are made by first growing tiny single crystals (size ≈ 50 µm) of CZTS in a molten KI salt solution at high temperature. These crystals are then embedded into a thin polymer layer on a substrate. A thin n-type CdS buffer layer is deposited on each grain to form a p–n junction, followed by conductive layers for charge collection. Finally, the structure Au/CZTS/CdS/i-ZnO/ZnO:Al is encapsulated to create a functional solar cell, where each grain acts as a miniature photovoltaic unit. More detailed description of the preparation of MG solar cells can be found in [9–11].

3. Results and discussion

The back contact formation differs significantly between the two types of solar cells. In TF cells, the Mo/MoS_2/CZTS interfaces is formed during the high-temperature sulfurization, whereas in MG cells, the p^+-layer is created by mechanically polishing the CZTS grains before the deposition of gold back contacts. The model for CZTS cell back contact is given in Fig. 2(a). In both situations, a particular kind of potential barrier is present. For actual physical processes, where potential barriers are typically defined by bell-like shapes, more straightforward potentials, such as rectangular or triangular, are not very suitable. We choose the modified Pöschl-Teller potential model for this reason. Naturally, this model has an analytical solution, which makes it more appealing than, say, a Gaussian potential barrier. Alternatively, tunneling processes in semiconductors can be calculated using the Eckart barrier model. [12] The Pöschl-Teller barrier has a shape $U(x) = U_0/\cosh\left(\frac{x}{a}\right)^2$, where $(U_0, a > 0)$, a is related to the width of the barrier, U_0 is the height of the barrier, see Fig. 2(b). This modified Pöschl–Teller potential barrier has a solution: [13–15]

$$T_R = \frac{\sinh^2\left(\pi\sqrt{2\epsilon}\right)}{\sinh^2\left(\pi\sqrt{2\epsilon}\right) + \cosh\left(\frac{\pi}{2}\sqrt{8u_0 - 1}\right)} \tag{1}$$

where $u_0 = m^* a^2 U_0/\hbar^2$ and $\epsilon = m^* a^2 E/\hbar^2$, m^* is a hole effective mass in CZTS ($m^* = 6.47{*}10^{-31}$ kg [16]), and $E = kT$ is a holes thermal energy, where k is the Boltzmann constant. T_R has values between 0 and 1, u_0 and ϵ are dimensionless parameters. In this case the temperature dependence of J_{SC} can be fitted with

$$J_{SC}(T) = J_{\min} + (J_{\max} - J_{\min}) * T_R(T) \tag{2}$$

where $J_{\min}$ and $J_{\max}$ are J_{SC} values at $T = 20$ and 320 K, respectively. A theoretical $T_R(T)$ shape with various barrier height U_0 values is displayed in Fig. 2(c). The experimentally measured S-shape curves and the T_R (T) shape are similar. Consequently, we fitted measured curves using Eq. 2. The fitting parameters are listed in Table 1, and the fitting results are shown as continuous lines in Fig. 1(b).

The *Jsc(T)* fittings in Fig. 1(b) exhibit significantly different $J_{\min}$ values at low temperatures, where the theoretical T_R approaches zero. This behavior suggests that the barrier height U_0 is not uniform, but instead follows a spatial distribution. The spatial distribution of barrier heights is clearly absent in a fully homogenous Schottky junction, and the $J_{SC}(T)$ curve will have longer horizontal sections close to Jmin and Jmax. The behavior of TF2 cell is a good example, see Fig. 1 (b). However, the spatial homogeneity of the junction will not have an impact on the barrier height determined by the fitting. For inhomogeneous back contact, it is simply an average barrier height. In Ref. [17], the spatial distribution of solar-cell properties in CZTSSe monograin solar cells was investigated using light-beam-induced current (LBIC) and electroluminescence (EL) measurements. The study showed that the spatial distribution of the generated current and the EL intensity follows a Gaussian profile. The same distribution function has been widely used to describe the spatial variation of barrier heights in inhomogeneous Schottky diodes. In this case, the barrier height is assumed to follow a Gaussian distribution:

$$P(\phi) = \frac{1}{\sigma\sqrt{2\pi}} \exp\left(-\frac{(\phi - \phi_0)^2}{2\sigma^2}\right), \tag{3}$$

where P is a probability, ϕ_0 is the mean barrier height, ϕ is a local barrier height, and σ is the standard deviation characterizing barrier-height fluctuations. Since the current preferentially flows through regions with lower barrier heights, an effective barrier height ϕ_{eff} can be

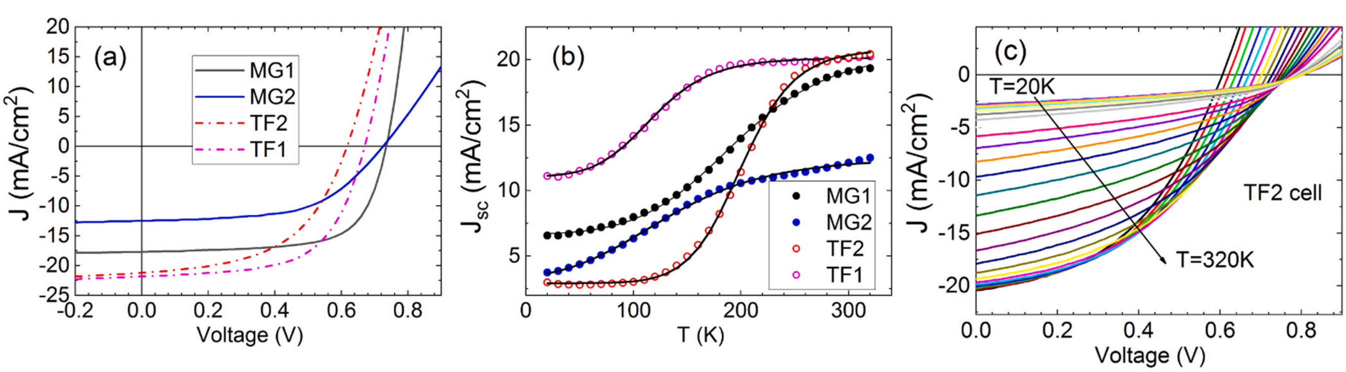

Fig. 1. (a) Room temperature *J-V* curves and (b) temperature dependence of J_{SC} for 4 different CZTS solar cells. The fitting result is shown as continuous lines. (c) Temperature dependent *J-V* curves of the TF2 cell.

Table 1
Parameters obtained from *J-V* curves and fitting parameters for all solar cells. The last column shows the quality of fitting (R^2 values).

Cell	η (%)	V_{OC} (mV)	FF (%)	J_{SC} (mA/cm^2)	U_o (meV)	a (nm)	J_{min} (mA/cm^2)	J_{max} (mA/cm^2)	R^2
MG1	9.0	735.4	69.0	17.7	59.2	2.4	6.7	19.6	0.9993
MG2	5.1	725.9	55.7	12.7	38.3	1.9	3.7	12.1	0.9978
TF1	8.9	670.3	61.3	21.8	35.8	3.2	11.1	20.1	0.9988
TF2	6.9	616.6	53.3	21.2	64.0	4.5	2.9	20.6	0.9994

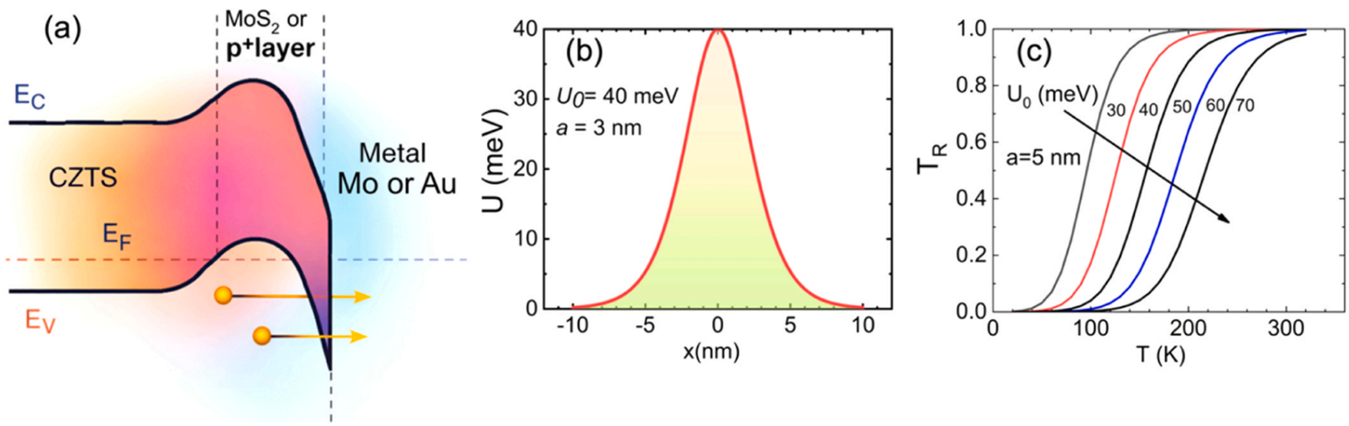

Fig. 2. Back contact model for CZTS solar cells (a); the shape of a potential barrier for holes in CZTS solar cells (b); calculated transmission T_R for different heights of the barrier (c).

defined: [18]:

$$\phi_{eff} = \phi_0 - \frac{q\sigma^2}{2kT}, \quad (4)$$

where q is the elementary charge, k is the Boltzmann constant, and T is the absolute temperature. According to Eq. 4, the effective barrier height decreases with decreasing temperature because charge transport becomes increasingly dominated by low-barrier regions. Conversely, at higher temperatures, the contribution of regions with different barrier heights becomes more uniform, causing ϕ_{eff} to approach the mean barrier height ϕ_0. The parameter σ, which determines the width of the Gaussian distribution, governs the temperature dependence of ϕ_{eff}: larger values of σ indicate greater barrier-height inhomogeneity and result in a more pronounced reduction of the effective barrier height at a given temperature. Barrier inhomogeneity can be caused by a variety of factors, including non-uniformity of the interfacial charges, grain boundaries, and compositional or potential fluctuations. [19–22] Larger values of the distribution width indicate more inhomogeneous junction properties. At low temperatures, regions with lower barriers dominate the current transport and give rise to J_{min}. Consequently, the current predominantly flows through these low-barrier regions, leading to non-zero J_{min} values. As the temperature increases, more carriers acquire enough energy to overcome higher barriers, resulting in an increase in J_{sc}. [20,23] Near room temperature, nearly all generated holes can penetrate the barriers, causing the J_{SC} behavior to exhibit a saturation; see Fig. 1(b). Although some extremely high barriers continue to affect hole tunneling at room temperature due to the Gaussian distribution of barrier heights, the TF cells exhibit nearly perfect saturation, as shown in Fig. 1(b). It means that MG cells have a wider distribution of barrier heights. Although we did not consider the temperature dependence of the series resistance Rs, barrier height, or the band gap energy E_g, the fitting results indicate that the hole transport at low temperatures of all cells may be affected significantly by quantum mechanical tunneling through the back-contact barrier, while at room temperature all cells approach ohmic behavior.

4. Conclusions

In conclusion, we investigated the temperature dependence of J_{SC} in various CZTS solar cells over the 20–320 K range to examine back contact behavior. All measured $J_{SC}(T)$ curves exhibited an S-shaped profile, which was analyzed using a modified Pöschl–Teller potential barrier model. The tunneling probability of holes through this barrier also displayed an S-like temperature dependence. The average barrier height was found to range from 36 to 64 meV. In addition, the experimental data can be satisfactorily described by assuming a Gaussian distribution of the back-contact barrier height. Such a distribution is physically plausible, as the barrier height is expected to vary spatially due to interface nonuniformities and irregularities at the back-contact interface. While all solar cells approach ohmic behavior at ambient temperature, hole tunneling through the rear contact barrier becomes important at temperatures below 300 K.

CRediT authorship contribution statement

Achmad Nasyori: Methodology. **Marit Kauk-Kuusik:** Writing – review & editing, Supervision, Resources. **Jüri Krustok:** Writing – original draft, Validation, Methodology, Data curation. **Raavo Josepson:** Investigation, Formal analysis.

Declaration of Competing Interest

The authors declare that they have no known competing financial interests or personal relationships that could have appeared to influence the work reported in this paper.

Acknowledgments

This work was supported by the European Union through the European Regional Development Fund (Project TK210U7). The research was carried out using the NAMUR + core facility, funded by the Estonian Research Council (Projects TT13, TTK26).

Data availability

Data will be made available on request.

References

[1] M.A. Green, E.D. Dunlop, M. Yoshita, N. Kopidakis, K. Bothe, G. Siefer, X. Hao, J. Y. Jiang, Solar cell efficiency tables (Version 67), Prog. Photovolt. Res. Appl. 34 (2026) 482–496, https://doi.org/10.1002/pip.70068.

[2] M. He, C. Yan, J. Li, M.P. Suryawanshi, J. Kim, M.A. Green, X. Hao, Kesterite solar cells: insights into current strategies and challenges, Adv. Sci. 8 (2021) 2004313, https://doi.org/10.1002/advs.202004313.

[3] C. Platzer-Björkman, N. Barreau, M. Bär, L. Choubrac, L. Grenet, J. Heo, T. Kubart, A. Mittiga, Y. Sanchez, J. Scragg, S. Sinha, M. Valentini, Back and front contacts in kesterite solar cells: state-of-the-art and open questions, J. Phys. Energy 1 (2019) 044005, https://doi.org/10.1088/2515-7655/ab3708.

[4] Y. Zhao, Z. Yu, J. Hu, Z. Zheng, H. Ma, K. Sun, X. Hao, G. Liang, P. Fan, X. Zhang, Z. Su, Over 12% efficient kesterite solar cell via back interface engineering, J. Energy Chem. 75 (2022) 321–329, https://doi.org/10.1016/j.jechem.2022.08.031.

[5] V. Karade, A. Lokhande, P. Babar, M.G. Gang, M. Suryawanshi, P. Patil, J.H. Kim, Insights into kesterite's back contact interface: a status review, Sol. Energy Mater. Sol. Cells 200 (2019) 109911, https://doi.org/10.1016/j.solmat.2019.04.033.

[6] M. Moustafa, T. AlZoubi, S. Yasin, Towards high-efficiency CZTS solar cells via p-MoS 2 interfacial layer optimisation, Mater. Technol. 37 (2022) 1563–1572, https://doi.org/10.1080/10667857.2021.1964214.

[7] A. Latreche, Combined thermionic emission and tunneling mechanisms for the analysis of the leakage current for Ga2O3 Schottky barrier diodes, SN Appl. Sci. 1 (2019) 188, https://doi.org/10.1007/s42452-019-0192-2.

[8] A. Nasyori, M. Pilvet, A. Saar, J. Krustok, M. Danilson, R. Kaupmees, V. Mikli, Y. Gong, R. Josepson, E. Saucedo, M. Grossberg-Kuusk, M. Kauk-Kuusik, ambient air processed Cu 2 ZnSnS 4 absorber layers from DMSO-based precursors: enhanced efficiency via device post-annealing, J. Mater. Chem. A 13 (2025) 30167–30179, https://doi.org/10.1039/D5TA04554A.

[9] M. Kauk-Kuusik, K. Timmo, K. Muska, M. Pilvet, J. Krustok, M. Danilson, V. Mikli, R. Josepson, M. Grossberg-Kuusk, Reduced recombination through CZTS/CdS interface engineering in monograin layer solar cells, J. Phys. Energy 4 (2022) 024007, https://doi.org/10.1088/2515-7655/ac618d.

[10] M. Kauk-Kuusik, K. Timmo, K. Muska, M. Pilvet, J. Krustok, R. Josepson, G. Brammertz, B. Vermang, M. Danilson, M. Grossberg, Detailed Insight into the CZTS/CdS interface modification by air annealing in monograin layer solar cells, ACS Appl. Energy Mater. 4 (2021) 12374–12382, https://doi.org/10.1021/acsaem.1c02186.

[11] M. Kauk-Kuusik, K. Timmo, M. Pilvet, K. Muska, M. Danilson, J. Krustok, R. Josepson, V. Mikli, M. Grossberg-Kuusk, Cu 2 ZnSnS 4 monograin layer solar cells for flexible photovoltaic applications, J. Mater. Chem. A 11 (2023) 23640–23652, https://doi.org/10.1039/D3TA04541B.

[12] M.V. Boev, V.M. Kovalev, O.V. Kibis, Optically induced resonant tunneling of electrons in nanostructures, Sci. Rep. 13 (2023) 19625, https://doi.org/10.1038/s41598-023-46998-w.

[13] E. Pöschl, G. Teller, Bemerkungen zur Quantenmechanik des anharmonischen Oscillators, Z. F. üR. Phys. 87 (1934) 364–369, https://doi.org/10.1007/BF01333431.

[14] F.M. Fernández, Quantum Gaussian wells and barriers, Am. J. Phys. 79 (2011) 752–754, https://doi.org/10.1119/1.3574505.

[15] J. Krustok, K. Timmo, M. Kauk-Kuusik, M. Grossberg-Kuusk, Tunneling-enhanced interface recombination and current loss curves in kesterite solar cells, Appl. Phys. Lett. 123 (2023), https://doi.org/10.1063/5.0175082.

[16] C. Persson, Electronic and optical properties of Cu2ZnSnS4 and Cu2ZnSnSe4, J. Appl. Phys. 107 (2010) 1–8, https://doi.org/10.1063/1.3318468.

[17] C. Neubauer, A. Samieipour, S. Oueslati, K. Ernits, D. Meissner, Spatially resolved opto-electrical performance investigations of Cu 2 ZnSnS 3.2 Se 0.8 photovoltaic devices, Energy Sci. Eng. 6 (2018) 563–569, https://doi.org/10.1002/ese3.232.

[18] J.H. Werner, H.H. Güttler, Transport properties of inhomogeneous Schottky contacts, Phys. Scr. T39 (1991) 258–264, https://doi.org/10.1088/0031-8949/1991/T39/039.

[19] I. Jyothi, H.-D. Yang, K.-H. Shim, V. Janardhanam, S.-M. Kang, H. Hong, C.-J. Choi, Temperature dependency of schottky barrier parameters of Ti Schottky contacts to Si-on-insulator, Mater. Trans. 54 (2013) 1655–1660, https://doi.org/10.2320/matertrans.M2013015.

[20] H. Li, D. He, Q. Zhou, P. Mao, J. Cao, L. Ding, J. Wang, Temperature-dependent Schottky barrier in high-performance organic solar cells, Sci. Rep. 7 (2017) 40134, https://doi.org/10.1038/srep40134.

[21] S. Chand, S. Bala, Analysis of current–voltage characteristics of inhomogeneous Schottky diodes at low temperatures, Appl. Surf. Sci. 252 (2005) 358–363, https://doi.org/10.1016/j.apsusc.2005.01.009.

[22] J.H. Werner, H.H. Güttler, Barrier inhomogeneities at Schottky contacts, J. Appl. Phys. 69 (1991) 1522–1533, https://doi.org/10.1063/1.347243.

[23] S. Toumi, Z. Ouennoughi, R. Weiss, Temperature analysis of the Gaussian distribution modeling the barrier height inhomogeneity in the Tungsten/4H-SiC Schottky diode, Appl. Phys. A 127 (2021) 661, https://doi.org/10.1007/s00339-021-04787-0.